Available online at www.sciencedirect.com
SCIENCE DIRECT®
Coordination Chemistry Reviews 249 (2005) 375–390
COORDINATION CHEMISTRY REVIEWS
www.elsevier.com/locate/ccr

Reactions of hydroxymethyl and hydride complexes in water: synthesis, structure and reactivity of a hydroxymethyl–cobalt complex

Carol Creutz*, Mei H. Chou, Etsuko Fujita, David J. Szalda[1]

Chemistry Department, Brookhaven National Laboratory, Upton, NY 11973-5000, USA

Received 9 February 2004; accepted 6 August 2004
Available online 2 December 2004

Contents

Abstract

The properties and reactions of hydroxymethyl and hydride complexes are surveyed with an emphasis on their aqueous chemistry; then the syntheses and reactions found for macrocyclic cobalt complexes of these ligands are presented. The hydroxymethyl–cobalt(III) complex

* Corresponding author. Tel.: +1 631 344 4359; fax: +1 631 344 5815.
E-mail address: ccreutz@bnl.gov (C. Creutz).
[1] Present address: Department of Natural Sciences, Baruch College, New York, NY 10010, USA.

0010-8545/$ – see front matter
doi:10.1016/j.ccr.2004.08.027

was prepared by addition of the photogenerated CH_2OH radical to the cobalt(II) macrocycle *N-meso*-$CoHMD^{2+}$ (HMD = 5,7,7,12,14,14-hexamethyl-1,4,8,11-tetraazacyclotetradeca-4,11-diene) in 0.1 M perchloric acid and characterized by an X-ray crystallographic study and spectroscopic characterization in solution. Acidic aqueous solutions are fairly stable and the complex decomposes, with formaldehyde elimination, by a base-catalyzed pathway. At 25 °C, formaldehyde elimination proceeds with the rate law $-d[N\text{-}meso\text{-}CoHMD(CH_2OH)^{2+}]/dt = k_I[N\text{-}meso\text{-}CoHMD(CH_2OH)^{2+}]/[H^+]$, with $k_I = (3.5 \pm 0.5) \times 10^{-9}$ M s^{-1} at pH 4–7 and 0.5 M ionic strength to yield the hydride complex, *N-meso*-$CoHMD(H)^{2+}$ and CH_2O. In a subsequent stage, *N-meso*-$CoHMD^{2+}$ and H_2 form with the rate law $-d[N\text{-}meso\text{-}CoHMD(H)^{2+}]/dt = (2 \pm 1) \times 10^{-7}$ $[N\text{-}meso\text{-}CoHMD(H)^{2+}]^2/[H^+]$ s^{-1} at pH 4.5–8 and 0.5 M ionic strength. Ultimately, the *N-meso* complex isomerizes to yield *N-rac*-$CoHMD^{2+}$ with previously observed kinetics.

Keywords: Hydroxymethyl complex; Hydride complex; Water reduction mechanism

1. Introduction

In parallel to the traditional organometallic chemistry of metal–carbon bonds is a rich aqueous chemistry, dominated by first transition-series metal ions [1–7]. Metal–carbon bonded species may result from the reaction of low valent, rather highly reducing metal centers (e.g, Ni(I)macrocycle [8] or an Fe(I)porphyrin [9]) with an alkyl halide. Cobalt–carbon bonds may be formed through the addition of carbon radicals to low-spin cobalt(II), typically chelated to a polyaza macrocycle [10–12]. The carbon radical may be generated chemically [13], photochemically [11,14] or via radiation chemistry techniques [15,16]. Of interest in the area of carbon dioxide reduction is the series of model complexes in which the carbon ligand is successively more reduced:

CoL($\mathbf{CO_2}$), CoL$\mathbf{CO}$, CoL($\mathbf{CHO}$) or CoL($\mathbf{CH(OH)_2}$),

CoL($\mathbf{CH_2OH}$), CoL($\mathbf{CH_3}$).

(cf. the analogous series of Ru(II) [17,18], η^5-C_5H_5Fe [19] complexes). With the macrocycle L = HMD = 5,7,7,12,14,14-hexamethyl-1,4,8,11-tetraazacyclotetradeca-4,11-diene, for which racemic and *meso* isomers exist,

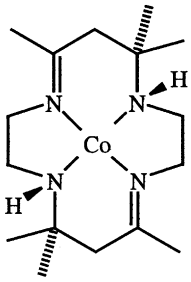

N-rac-CoHMD

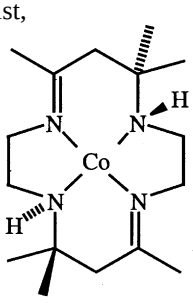

N-meso-CoHMD

the first [20,21], second [22] and last [23] members of the series have been described. Here, the fourth member of the series, the hydroxymethyl complex, conjugate acid of the (cobalt(I)) formaldehyde complex, is reported for the *N-meso* HMD isomer. In addition to the chemistry exhibited by the hydroxymethyl complex studied here, the system is of interest because it provides access to information about the cobalt(III) hydrides of this family [24,25] and the pathway for their reaction to form dihydrogen in water [26], which is important in applications such as the photoreduction of water [27]. Such pathways have been examined to only a very limited extent [28].

1.1. Previously characterized hydroxymethyl complexes

The complex $HOCH_2Co(CO)_4$ has been proposed as an intermediate in the reaction of formaldehyde with $HCo(CO)_4$ to produce $HOCH_2CHO$ [29]. Since 1980, several organometallic hydroxymethyl complexes have been characterized. The first was η^5-$C_5H_5Re(CO)(NO)CH_2OH$ [30]. Metallacycle-stabilized, α-hydroxyalkyl species have been explored by Vaughn and Gladysz [31,32]. Re(bpy)$(CO)_3(CH_2OH)$ (bpy = 2,2′-bipyridine), prepared by borohydride reduction of the tetracarbonyl compound, has been characterized [33]. Borohydride reduction of the metallacarbonyl was also used to synthesize $C_5(CH_3)_5Fe(CO)_2CH_2OH$ [34] and $Ru(bpy)_2(CO)CH_2OH$ [17]. The hydroxymethyl complexes of rhodium octaethylporphyrin [35] and Rh(dbpb) (dbpb = 4,5-dimethyl-1,2-bis((4-(1-butylpentyl))pyridine-2-carboxamido)benzene) [36] were prepared by reaction of hydrides with formaldehyde. Recently, the reactivity and thermodynamic studies of tetra-*p*-sulfonatophenyl porphyrin rhodium hydride ($[(TSPP)Rh–H]^{4-}$) with CO, aldehydes and olefins that produce formyl, α-hydroxyalkyl and alkyl complexes have been reported for water and compared with the related reactions in non-aqueous media [37,38]. The available ^{1}H NMR data for the organometallic species are summarized below.

In contrast to the organometallic species noted above, which are produced via BH_4^- reduction of bound CO or reaction of a metal hydride with formaldehyde, there are a number of hydroxymethyl complexes formed from the addition of the organic radical $^\bullet CH_2OH$ to a first transition-series metal center M [39–43].

$$LM^{II} + R^\bullet \underset{k_{-1}}{\overset{k_1}{\rightleftharpoons}} LM^{III}\text{–R} \quad (1)$$

The addition rate constants are generally quite large (see Table 2).

In the above pulse-radiolysis experiments, the hydroxymethyl radical was generated from the reaction of methanol with hydroxyl radical. For synthetic purposes photochem-

Table 1
^{1}H NMR data for hydroxymethyl complexes

Species	Solvent	δ	Reference
$H_2C(OH)(OCH_3)$ hemiacetal	CH_3OH	4.64	[33]
H_2CO	CH_3OH	9.50	[33]
$Re(bpy)(CO)_3CH_2OH$	CH_3OH	3.37 s, 2H	[33]
	CD_3CN	3.27 s, 2H[a] ^{13}C 69.4[a]	
$Ru(bpy)_2(CO)CH_2OH$	CD_3CN	4.34, 4.37; 4.45, 4.47; J = 7.24 Hz {270 MHz}	[17]
$Rh(oep)CH_2OH$[b]	C_6D_6	−2.34	[35]
$\{Rh(oep)CH_2\}_2O$ (ether)[b]	C_6D_6	−2.44	[35]
$(dbpb)RhCH_2OH$	THF	5.14 (*d* of *d*)	[36]
$C_5(CH_3)_5Fe(CO)_2CH_2OH$	THF	4.02[3]; J = 3 Hz	[34]

[a] E. Fujita, unpublished work.
[b] oep: octaethylporphyrin.

ical decomposition of another metal complex containing the $^{\bullet}CH_2OH$ fragment can be used, for example photolysis of $HOCH_2Co(dmgBF_2)_2$ (dmg = dimethylglyoximate) in the presence of [14]-aneN$_4$ [13] or, as used in the present work, UV photolysis [14] of $Co(NH_3)_5OC(O)R^{2+}$ to generate the R = $^{\bullet}CH_2OH$ radical in the presence of *N-meso*-$CoHMD^{2+}$ [44,45]. Chemical methods have been widely used as well. For $Cr(H_2O)_5CH_2OH^{2+}$, the radical was produced from the reaction of hydroxyl radical with methanol, with hydroxyl radical in turn produced by the reaction of chromium(II) with hydrogen peroxide [42].

Transalkylation, the transfer of R$^{\bullet}$ from one metal center to another [4,46], was used to prepare $HOCH_2Co(dmgBF_2)_2$ [46] (via alkyl transfer from Cr–R).

$$M_1R^{2+} + M_2{}^{2+} \rightarrow M_1{}^{2+} + M_2R^{2+}$$

In addition, the hydroxymethyl complex of bis(diacetyldioximato)cobalt has been described [47].

In general, methyl complexes seem to be the most stable of the alkyl complexes with respect to homolysis, followed by hydroxymethyl, but as is evident from Table 2, there are very large differences between the absolute stabilities of the different series of aliphatic complexes.

1.2. Reaction pathways for hydroxymethyl complexes in water

Decomposition pathways recorded for hydroxymethyl complexes in water include reductive elimination, homolysis, heterolysis, and displacement.

1.2.1. Reductive elimination of formaldehyde

In pulse-radiolysis studies, *racemic* $CoHMD(CH_2OH)$ yielded formaldehyde, with a first-order rate constant of 0.1 s^{-1} invariant with pH [39]:

$$rac\text{-}Co(HMD)CH_2OH^{2+} + H_2O \rightarrow rac\text{-}Co(HMD)^{+} + CH_2O + H_3O^{+}, \text{ neutral pH}$$

$$rac\text{-}Co(HMD)CH_2OH \rightarrow rac\text{-}Co(HMD)H^{2+} + CH_2O, \text{ pH 1–2}$$

Preliminary observations indicated that the $dmgBF_2$ complex also decomposed by formaldehyde elimination, with formation of a metal hydride [46]:

$$HOCH_2Co(dmgBF_2)_2 \rightarrow HCo(dmgBF_2)_2 + CH_2O$$

1.2.2. Homolysis

In contrast to the above decomposition behavior (elimination of formaldehyde) polyaminocarboxylate cobalt–R complexes yield R–R. In the nitrilotriacetate (NTA) system, the reaction pattern consists of the sequence shown below.

$$LM^{II} + R^{\bullet} \underset{k_{-a}}{\overset{k_a}{\rightleftharpoons}} LM^{III}\text{–}R$$

$$LM^{III}\text{–}R + R^{\bullet} \xrightarrow{k_b} LM^{II} + R\text{–}R$$

The radical is bound to the Co^{II}NTA. The decay of this adduct is second-order in the adduct and inhibited by Co^{II}NTA, a rate law consistent with attack of the free rad-

Table 2
Rate constants for addition of hydroxymethyl radical to M−L in water at 298 K[a]

M–L	k_1 (M^{-1} s^{-1})	k_{-1} (s^{-1})	K_1 (M^{-1})	Reference
rac-$Co(HMD)(H_2O)^{2+}$	7×10^7	$<10^{-1}$	$>10^8$	[39]
$Co(NTA)(H_2O)^{-}$	2.0×10^8	3.9×10^4	5.1×10^3	[40]
$Co(Hedta)(H_2O)^{-}$	1.2×10^7	<60	$>2 \times 10^5$	[40]
$Cr(H_2O)_5{}^{2+}$	1.6×10^8	3.7×10^{-5}	4.3×10^{12}	[41,42]
trans-[15]ane-$N_4Cr(H_2O)^{2+}$	1.2×10^8	$<2 \times 10^{-2}$	$>6 \times 10^9$	[43]
cis-$Cr(NTA)(H_2O)^{-}$	2.2×10^8			[43]

[a] NTA: nitrilotriacetate, edta: ethylenediaminetetraacetate.

ical R• on the bound radical Co^{III}NTA–R to give R–R as product. Evidently polyaminocarboxylate ligands do not provide the stabilization of low-oxidation state metals (e.g., Co(I)) needed for the elimination process to occur. (Analogous R–R forming pathways have been found for Cu(II) glycinate complexes with R = CH_3 [48] and for NTA complexes of Mn(II) and Fe(II) [49].) Depending on the metal center and ligand set acidolysis to yield the alkane, R–H may occur in parallel (see below). However, for the case of $HOCH_2Co(NTA)(H_2O)^-$, acidolysis is negligible and only $(HOCH_2)_2$ is formed [40]. Remarkably, similar rate constants ($2k = 1 \times 10^9\ M^{-1}\ s^{-1}$) were inferred for dimerization of hydroxymethyl radical via reaction of the free radical with $HOCH_2Co(NTA)(H_2O)^-$, $OCH_2Co(NTA)(H_2O)^{2-}$, and with $HOCH_2$•. $HOCH_2Co(hedta)(H_2O)$ decayed by a different pathway that was not characterized [40].

1.2.3. Acidolysis/heterolysis

The aquachromium complex decays by acidolysis with $k = 6.6 \times 10^{-4} + 4.65 \times 10^{-4}\ [H_3O^+]\ s^{-1}$, corresponding to contributions from HA = H_2O and H_3O^+, respectively [4].

$$LM^{III}\text{–}R + HA \xrightarrow{k_c} LM^{III} + R\text{–}H + A^-$$

For the edta analogue $Cr(edta)^-$ the acid dependent contribution is enhanced by more than a million compared to the acid-independent term [50].

The pK_a of $HOCH_2Co(NTA)(H_2O)^-$ is 4.7; that of $HOCH_2Co(hedta)(H_2O)$ is 9 [40]. Since no comparable pK value is obtained for the other alkyl radical adducts, it is ascribed to ionization of the hydroxymethyl group (rather than the trans water molecule).

1.2.4. Homolytic displacement reactions

As noted earlier, $HOCH_2$• can be transferred from one metal center to another [46].

$$Cr(H_2O)_5CH_2OH^{2+} + Co(dmgBF_2)_2 \rightarrow Cr(H_2O)_6^{2+} + HOCH_2Co(dmgBF_2)_2 \text{[46]}$$

1.3. Previously characterized hydride complexes in water

Metal hydride complexes may be generated in aqueous media by addition of H atom,

$$Cr(H_2O)_6^{2+} + H^\bullet \rightarrow Cr(H_2O)_5H^{2+}$$

[51] by reaction with dihydrogen

$$Co^{II}(Hdmg)_2py + 1/2H_2 \rightarrow HCo^{III}(Hdmg)_2py$$

[52–54] or by proton transfer to a reduced metal center.

$$Co^{II}(CN)_5^{3-} + e^- \rightarrow Co^{I}(CN)_5^{4-}$$

$$Co^{I}(CN)_5^{4-} + H_2O \rightleftarrows HCo^{III}(CN)_5^{3-} + OH^-$$

All are formally oxidative addition reactions since the hydride is by definition oxidation state −1 and the product metal centers exhibit properties expected for the oxidized metal center. Proton transfer reactions of metal hydrides in non-aqueous solvents have been extensively characterized by Kristjánsdóttir and Norton [55,56] and DuBois and coworkers have extensively characterized their thermodynamics in organic media [57–59]; most of the few data that exist for aqueous media were determined by pulse radiolysis [16,25,53]. The rate constants for protonation of cobalt(I) macrocycles

$$Co(HMD)^+ + HA \rightarrow Co(HMD)(H)^{2+} + A^-$$

increase with the pK_a of HA (see Table 3) (and with pressure [60]) and the rate constants for the deprotonation of the hydride by A^- decrease with the pK_a of HA.

The rate law for formation of $HRh(dmgH)_2P(C_6H_5)_3$ from its Rh(I) conjugate base contains terms for protonation by HA = water, buffer, and hydronium ion [61].

The formation of $Co(bpy)_2H^{2+}$ (bpy = 2,2′-bipyridine) occurs by reaction of the organic free radical bpyH with a bpy complex [62].

While there is generally little known about the reactions of more traditional organometallic hydrides in water, water-soluble species are beginning to be addressed [63,64]. Nickel complexes have been designed [57] that provide a model for hydrogenase activity [65].

1.4. Mechanisms of dihydrogen formation from hydride complexes

Of particular interest here is the detailed pathway for H_2 formation. The subject has been addressed in recent years [28] because of its importance in solar photoconversion [66]. Work prior to 1972 is covered by James [67]. For homogeneous systems, H_2 formation or H_2 activation, its microscopic reverse, is known [67,68] to occur by a homolytic mechanism, e.g.,

$$2HCo^{III}(CN)_5^{3-} \rightarrow H_2 + 2Co^{II}(CN)_5^{3-} \text{[69, 70]}$$

and by oxidative addition/reductive elimination involving a dihydride (and probably a dihydrogen complex [71,72]), e.g. [73]

$$Rh(bpy)_2(H)_2^+ \underset{24\ M^{-1}\ s^{-1}}{\overset{1.7\times10^{-2}\ s^{-1}}{\rightleftharpoons}} H_2 + Rh(bpy)_2^+$$

as seen in the following [74]

$$(P(C_6H_{11})_3)_2W(CO)_3(H)_2 \rightleftarrows H_2 + (P(C_6H_{11})_3)_2W(CO)_3 \rightleftarrows (P(C_6H_{11})_3)_2W(CO)_3(H_2)$$

and by heterolytic processes, e.g.,

$$(H_2O)_5CrH^{2+} + H_3O^+ \rightarrow (H_2O)_6Cr^{3+} + H_2 [51, 75],$$
$$k = 1.0 \times 10^4\ M^{-1}\ s^{-1}$$

(The latter may involve transient dihydrogen or dihydride complexes, as well.) For the case of $HCo(dmgH)_2P(n\text{-}C_4H_9)_3$ (dmg = dimethylglyoximato), there is evidence for parallel homolytic and heterolytic paths [76]. $Co(dmgBF_2)^{2+}$ catalyzes the formation of H_2 from solutions of reducing agents such as Eu(II), Cr(II), and V(II) [77]. The formation of H_2 from $HRh(dmgH)_2P(C_6H_5)_3$ was attributed to a heterolytic process [61]. The mechanism for H_2 formation in the photochemical, ascorbate-driven, CoHMD/$Ru(bpy)_3^{2+}$ system has not been determined [26]. Rhodium(III) complexes containing $(CH_3)_5C_5^-$ and a 2,2′-bipyridyl derivative as ligands are active catalysts for photochemical hydrogen formation; protonation of a Rh(I) hydride is implicated as the rate-determining step [28,78,79]. In particularly elegant work DuBois and co-workers have designed nickel phosphine (e.g., $Et_2PCH_2N(Me)CH_2PEt_2$ = PNP) complexes with hydrogenase-like activity in that they offer H^+ and H^- binding sites, N and Ni(II), respectively, for the binding of H_2 [58].

There are now several systems in which reduction of a metal hydride is evidently required for dihydrogen to be formed. In the original photochemical [80] system based on $Ru(bpy)_3^{2+}$, $Rh(bpy)_3^{3+}$, triethanolamine and $PtCl_6^{4-}$, H_2-formation was catalyzed by colloidal Pt [81,82]. However, homogeneous catalysis by $HRh(bpy)_2^+$, a Rh(II) hydride, formed by reduction of the Rh(III)–H by $Rh(bpy)_3^{2+}$, was implicated in radiolysis studies of dihydrogen formation [83,84]. The $Rh(bpy)_3^{2+}$ (E^0 −0.86 V versus NHE [85]) formed by photochemical or radiolytic reduction of the Rh(III) complex is the precursor of $Rh(bpy)_2^{2+}$ and its reductant:

$$Rh(bpy)_3^{3+} + e^- \rightarrow Rh(bpy)_3^{2+}$$

$$Rh(bpy)_3^{2+} \rightleftharpoons Rh(bpy)_2^{2+} + bpy$$

$$Rh(bpy)_2^{2+} + Rh(bpy)_3^{2+} \rightarrow Rh(bpy)_2^{+} + Rh(bpy)_3^{3+}$$

$$Rh(bpy)_2^{+} + H_3O^+ \rightleftharpoons Rh(bpy)_2(H_2O)(H)^{2+}$$

$$pK_a = \sim 7.5 [83, 86]$$

$$Rh(bpy)_3^{2+} + Rh(bpy)_2(H)^{2+} \rightarrow Rh(bpy)_3^{3+} + Rh(bpy)_2(H)^+$$

$$Rh(bpy)_2(H)^+ \rightarrow\rightarrow Rh(bpy)_2^{2+} + H_2$$

The mechanism by which the Rh(II)–H reacts to give H_2 is not known, and could be either homolytic or heterolytic [83,84]. It is noteworthy that the further reduced species $Rh(bpy)_2(H)_2^+$ is in equilibrium with H_2 and $Rh(bpy)_2^+$ in acetone and that these could be formed via disproportionation of $Rh(bpy)_2(H)^+$ [73].

Catalysis and electrocatalysis of hydrogen formation by cobaltocene [87] and phosphine derivatives such as $(C_5H_5)Co(P(OCH_3))_2$ [88] requires reduction of the cobalt(III) hydride initially generated via reduction of cobalt(II) to cobalt(I), followed by its protonation to the cobalt(III) hydride.

$$(C_5H_5)LCo^{II} + e^- \rightarrow (C_5H_5)LCo^{I}$$

$$(C_5H_5)LCo^{I} + H^+ \rightarrow (C_5H_5)LCo^{III}H$$

$$(C_5H_5)LCo^{III}H + e^- \rightarrow (C_5H_5)LCo^{II}H$$
$$\rightarrow\rightarrow (C_5H_5)LCo^{II} + H_2$$

As above, the mechanism by which the Co(II)–H reacts to give H_2 is not known, and could be either homolytic or heterolytic. At the electrode, the above sequence is said to be an ECE mechanism (the formation of the hydride is the chemical step). When the reaction involves only the homogeneous system, the second "e" is provided by Co(I). A similar mechanism has been observed for a rhodium porphyrin system [89], with slight differences because the Rh(II) oxidation state (in contrast to Co(II)) is not stable. Addition of axial ligand triphenyl phosphine activates the Rh(III)–H so that H_2 is formed through the reactions of both Rh(II)–H and Rh(III)–H with acid. The mechanism found for an iron porphyrin system has the same key features (except that more electrons are needed to reach the catalytically active hydride [90]).

All of these systems require the reduction of a d^6 M − H species to a d^7, 19-electron species for activity. Thus, catalysis occurs via Co(II)–H, Rh(II)–H, and Fe(I)–H species.

1.4.1. Overriding issues in H_2 formation

Any couple with E^0_M or E^0_M more negative than that of hydrogen $E^0_{H^+}$ under the prevailing conditions is thermodynamically capable of reducing water to hydrogen.

$$M^{III} + e^- \rightarrow M^{II} \quad E^0_{M^{III/II}}$$

$$M^{III} + 2e^- \rightarrow M^{I} \quad E^0_{M^{III/I}} = \tfrac{1}{2}(E^0_{M^{III/II}} + E^0_{M^{II/I}})$$

$$M^{II} + e^- \rightarrow M^{I} \quad E^0_{M^{II/I}}$$

$$\tfrac{1}{2}H^+ + e^- \rightarrow H_2 \quad E^0_{H^+}$$

While the potential needed for hydrogen ion reduction shifts 0.059 V per pH unit, the driving force for homolytic H_2 formation from a hydride complex via

$$MH^{2+} \rightleftharpoons M^{2+} + \tfrac{1}{2}H_{2(g)} \qquad K(MH/H_2) = \frac{[M^{2+}]P_{H_2}^{1/2}}{[MH^{2+}]}$$

Table 3
Rate constants for *N-meso*-CoL_5^{+} reactions[a]

Reactant	k ($M^{-1}\,s^{-1}$)
H_3O^+	2.3×10^9
HCO_2H	1.8×10^8
CH_3CO_2H	0.8×10^8
$H_2PO_4^-$	1.2×10^8
N_2O	1.0×10^7

[a] Aqueous solutions, 25 °C, various ionic strengths, from [25].

is independent of pH (provided, of course, that the dominant form of both the hydride and M^{2+} is pH-independent).

Kellet and Spiro have considered the thermodynamics of homolysis and heterolysis as elementary steps for cobalt porphyrins and concluded that homolysis ($\Delta G^0_{hom} = e(E^0_M - E^0_{H^+})$) is favored over heterolysis ($\Delta G^0_{het} = e(\frac{1}{2}(E^0_M + E^0_M) - E^0_{H^+})$) because of the high value of the Co(III)–Co(II) reduction potential [91]. Depending upon the system the kinetics and thermodynamics of formation of the hydride complex may be critical. For finite homogeneous rates, binding of the proton to the metal center is necessary to lower the barrier to H_2 formation. However, to the extent that the metal hydride adduct is stabilized, the formation of dihydrogen becomes less thermodynamically favorable. Within homologous series, the pK_a's of metal hydrides

$$MH^{2+} \rightleftharpoons M^+ + H^+ \quad pK_a(MH)$$

increase as the E^0_M or E^0_M become more negative. Thus, the result of an effort to increase the driving force for H_2 formation by making the metal couple more reducing can result in also increasing pK_a(MH) [92], which in part (or even entirely) mitigates the progress made. This trend is evident for the cobalt hydrides in Table 4.

Thus formation of the hydride from hydrogen gas and pentacyanocobaltate(II) is favored because of the very low acidity of the hydride, while in the cobaltocene system, for which the cobalt(I) couple is much less reducing, reduction of water to hydrogen is strongly favored because of the very high acidity of the cobalt hydride.

2. Experimental

2.1. Preparation of $CoHMD(CH_2OH)(H_2O)(ClO_4)_2$

UV photolysis [14] of $Co(NH_3)_5OC(O)R^{2+}$ was used to generate the R = $^{\bullet}CH_2OH$ radical in the presence of *N-meso*-$CoHMD^{2+}$ [44,45]. A volume of 100 mL of 0.1 M perchloric acid containing 82 mg $Co(NH_3)_5(OC(O)CH_2OH)(ClO_4)_2$, prepared from $Co(NH_3)_5(H_2O)(ClO_4)_2$ and hydroxyacetic acid [95], was bubbled with argon for 45 min. Then, 57.6 mg of *N-meso*-$CoHMD(ClO_4)_2$ was added. The solution was irradiated for 5 min with light from a Hanovia mercury lamp. The product solution was then reduced in volume to 15 mL on a rotary evaporator. The concentrate was transferred to a deaerated vessel (1 atm Ar) containing 2 g $NaClO_4$ and stored in a freezer overnight. The next day ~22 mg of solid perchlorate salt of the desired complex was collected on a glass frit, washed with ether, and dried in a vacuum desiccator. Anal.: Co 10.1%, ClO_4^- 32 ± 1%; calc.: Co 10.1%, ClO_4^- 33.9%. (Caution: perchlorate salts used in this study may be explosive and potentially hazardous.) ^{1}H NMR in D_2O/0.1 M D^+: –C**H**$_2$OH δ 3.58(1H, *d* of *d*, J = 26.6 and 2.8 Hz) and δ ~3.9 (1 H, overlapped with two protons of HMD). ^{13}C NMR in D_2O/0.1 M H^+: δ 61.6. IR (ν, cm^{-1}, KBr pellet): 3400 m (O–H), 3180 s (N–H), 3000, 2990 m (C–H), 1660 (C=N), 1500–1300 multiple macrocycle bands; 1100, 700 s (ClO_4^-).

2.2. Kinetics runs

A 1-cm UV–vis cuvette, topped with a serum-capped stopcock, was charged with 2.4 mL of aqueous acid or buffer of the desired composition. The cells were bubbled with argon to remove O_2, brought to 25 °C, and injected with 0.1 mL stock $[CoHMD(OH_2)(CH_2OH)](ClO_4)_2$, prepared by dissolving the solid in 0.01 M $HClO_4$ under Ar.

2.3. Analyses

H_2 in the head space of cuvettes in which the kinetics were followed spectrophotometrically was determined by GC on molecular sieve 5A (Ar carrier) [96]. Typically 100 μL samples were withdrawn from the ca. 3 mL headspace. Formaldehyde was determined spectrophotometrically with use of the chromotropic reagent [97]. To remove the CoHMD complexes, which can interfere with accurate CH_2O determination, 2.5 mL of the spent reaction mixture (from the cuvette in which the kinetics were monitored) was loaded onto a 1 cm × 10 cm column of Sephadex C-25 resin (H^+ form). The resin was washed with 10 mL water to remove the formaldehyde and the eluate was analyzed as described elsewhere [96].

2.4. Crystal structure determination

Diffraction data were collected with an Enraf-Nonius CAD-4 diffractometer at 296(2) K. $[Co(N_4C_{16}H_{32})(OH_2)(CH_2OH)](ClO_4)_2$ crystallizes as reddish orange, elongated trapezoids. A crystal of 0.22 mm × 0.22 mm × 0.42 mm was used for data collection. It exhibited monoclinic symmetry with systematic absences $0k0$, $k = 2n + 1$, consistent with space groups $P2_1$ C_2^2 (no. 4) and $P2_1/m$ C_{2h}^2 (no. 11) [98]. E-statistics indicated $P2_1$ as the correct space group and the subsequent solution and refinement of the structure confirmed this choice. Crystal data and details of data collection and reduction are given in Table 5.

Table 4
Thermodynamics of H_2 formation from metal hydride complexes near 298 K

Hydride complex	pK_a (MH)	$E^0_{M^{II/I}}$ (V)	log K ($M-H/H_2$) (atm$^{1/2}$)
$HCo^{III}(CN)_5^{3-}$	20 [53,54]	ca. −1.0 [54]	−0.96[a]
rac $HCo(HMD)^{2+}$	11.5 [25,93]	−1.36 [93]	11.6[b]
meso $HCo(HMD)^{2+}$	<12.8 [25,93]	−1.35 [25,93]	10.1[b,c]
$Co(bpy)_2(H_2O)H^{2+}$	6.9 [62]	−1.09 [94]	11.6[b]
$Co(C_5H_5)_2H^{2+}$	−1 [87]	−0.85 (vs. sce, CH_2Cl_2) [88]	15.4[b]

[a] Calculated from the equilibrium data reported originally as $2MH^{2+} \rightleftharpoons 2M^{2+} + H_{2(g)}$, $K = [H_2][M^{2+}]^2/[MH^{2+}]^2 = 6.6 \times 10^{-6}$ M using the H_2 solubility 0.6 mM/atm reported [70].
[b] Calculated from the tabulated values of pK_a(MH) and $E^0_{M^{II/I}}$; $\log(K) = -(0.059pK_a(MH) + E^0_M)$.
[c] Upper limit derived from isomer stabilities reported in [25,93].

2.5. Determination and refinement of the structure

The structure was solved by heavy atom Patterson methods. In the course of the solution and refinement of this structure a disordered model had to be introduced for the axial hydroxymethyl and water ligands and for the chlorine of one of the perchlorate anions. This disorder introduced a pseudo inversion center into the cation. Attempts to refine the structure in a centrosymmetric space group were not successful. The bond lengths to the two disordered axial groups were not significantly different, 2.191(12) and 2.167(10). Anisotropic temperature parameters were used for all the non-hydrogen atoms. All of the hydrogen atoms were placed in calculated positions and allowed to "ride" on the atom to which they were attached. The hydrogen atom on the oxygen of the disordered hydroxymethyl ligand was not included. A common isotropic thermal parameter was refined for the hydrogen atoms included in the refinement ($U = 0.093(6)$).

Table 5
Crystallographic data from the X-ray diffraction study of $[Co(N_4C_{16}H_{32})((OH_2)(CH_2OH)](ClO_4)_2$

Compound	$[Co(N_4C_{16}H_{32})(OH_2)(CH_2OH)](ClO_4)_2$
Formula	$C_{17}H_{37}Cl_2CoN_4O_{10}$
Molecular weight	587.34
Space group	$P2_1$
a (Å)	8.068(1)
b (Å)	17.403(1)
c (Å)	9.1820(9)
β (°)	106.95(1)
V (Å^3)	1233.2(1)
Z	2
ρ (calculated) (g cm^{-3})	1.582
Temperature (K)	296(2)
Radiation	Cu Kα
μ (mm^{-1})	7.973
Absorption correction max (min)	0.3289, 0.1537
Reflections collected	5226
Unique reflections ($F_o > 0$)	2733
Reflections/restraints/parameter	2733/0/335
θ limits (°)	5–75
R_1, wR_2 ($I > 2\sigma(I)$)	0.0681, 0.1727
R_1, wR_2 (all data)	0.1468, 0.2197
Max. shift/error, final cycle	≤0.045

$R_1 = \Sigma||F_o| - |F_c||/\Sigma|F_o|$; $wR_2 = \{\Sigma[w(|F_o^2| - |F_c^2|)^2]/\Sigma[|wF_o^2|^2]\}^{1/2}$.

3. Results

3.1. Structure of the hydroxymethyl compound

A view of the hydroxymethyl complex in $CoHMD(CH_2OH)(H_2O)(ClO_4)_2$ is given in Fig. 1. The numbering scheme for HMD is as has been used previously [22]. The metal center is six coordinate, with the four nitrogens of the macrocycle defining an equatorial plane and axially ligated water and the carbon of the hydroxymethyl completing the cobalt coordination sphere. The macrocycle is in the *N-meso* form [99], with the amine hydrogens of N1 and N8 on opposite sides of the macrocycle plane. The axial ligands are disordered resulting in pseudo $\bar{1}$ symmetry for the cation.

The average Co–N (amine) bond distance of 1.980(12) Å and Co–N (imine) bond distance of 1.928(12) Å are similar to those in previously reported structures [22,23,45,100,101]. Bond distances and angles involving the macrocycle are similar to those in previously characterized Co(II) and (III) complexes of the macrocycle [22,23,45]. The dihedral "fold" angle between the planes formed by N1, N8, N4 and N1, N8, and N11 is 1.0(8)°. The cobalt is 0.010(8) Å out of the plane formed by the four nitrogen atoms.

In complexes of the type $CoHMDX_2^{n+}$, where the axial X-ligands are identical, the complex contains a center of inversion. The complex reported here nearly contains such a center, as a result of the disordering of the axial ligands. This

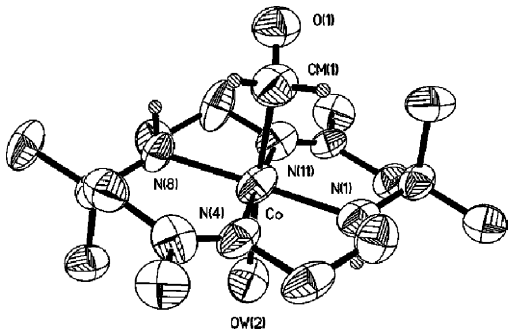

Fig. 1. A view of the cation of **1**. Thermal ellipsoids are at the 50% level and all hydrogen atoms except those on the amines of the macrocycle and the two methylene hydrogen atoms on the hydroxymethyl ligand are omitted for clarity. The cation has pseudo inversion symmetry which is reinforced by the disordering of the axial ligands. The CM(1)–Co–OW(2) angle is 175.3°.

disorder makes it impossible to determine whether or not the $-CH_2OH$ is configurationally disordered [18] as indicated by solution ^1H NMR spectra (vide supra).

The axial methyl groups of the macrocycle make close contacts with the axial ligands. The C(axial methyl)–axial (hydroxymethyl or water) distance is 3.23(2) Å and the C(axial methyl)–O(water) distance is 3.21(2) Å compared to a C(methyl)–C(methyl) distance of 3.46 Å in the secondary isomer of $CoHMD(CH_3)(OH_2)^{2+}$ and a C(methyl)–O(water) distance of 3.20 Å in the primary isomer [100]. The Co–C(hydroxymethyl) and Co–O(water) distances, 2.191(12) and 2.167(10) Å, respectively, are much longer (2.179 Å average) than found for primary or secondary *rac* $CoHMD(CH_3)(OH_2)^{2+}$ (1.977(8), 2.089(5) and 1.971(6), 2.115(4) Å).

The crystal lattice is held together by hydrogen bonds between the perchlorate anions and the N–H groups of the macrocycle amine functions and the axially coordinated hydroxymethyl and water molecules. Within the complex, there are intramolecular N–H···O hydrogen bonds: $N(1)\cdots OH_2$, 2.77(2) Å, and $N(8)\cdots OCH_2$, 3.29(2) Å.

3.2. Overview of the reactivity of *N-meso*-$CoHMD(CH_2OH)^{2+}$

The complex is formed by addition of the hydroxymethyl radical to the cobalt(II) complex in aqueous acid and is quite unreactive at high acid. When acidic stock solutions are diluted into buffers at various pH values and the spectra of the solutions are followed with time, three overall reaction stages are observed, all with rates inversely proportional to the acid concentration. The time evolution of the system is illustrated in Fig. 2.

In the first stage, as observed at pH 3–7, the visible absorption maximum shifts from 475 to 440 nm and formaldehyde is formed. The cobalt product is assigned as the hydride complex *N-meso*-$CoHMD(H)^{2+}$ [25]. In the second stage, the visible absorption band decreases in intensity, the maximum shifts from 440 to 446 nm and H_2 is formed. In the very slow third stage, the spectroscopic changes are identical with those reported earlier for isomerization of *N-meso*-$CoHMD^{2+}$ to *N-rac*-$CoHMD^{2+}$ [45]. Thus, the second stage forms *N-meso*-$CoHMD^{2+}$, along with the H_2. The first and third stages are first order in the cobalt complex, but the second stage, monitored through absorbance changes or hydrogen formation, is second-order with respect to the cobalt complex. The overall reaction scheme is summarized in Scheme 1.The spectral changes are illustrated in Fig. 2 and Table 6.

3.3. Rate and product data

Product yields and rate data obtained for aqueous solutions at low ionic strength are summarized in Tables 7 and 8, and for 0.5 M ionic strength, in Tables 8 and 10.

Most of the experiments were carried out in 1-cm cuvettes topped with stopcocks closed with serum caps (runs 1–5, 7–24) and reaction was initiated by injecting a small volume of stock solution into buffer. In run 6, the ^1H NMR spectrum was followed with time. In initial runs in formate (#4) and CO_2 saturated HCO_3^- buffer (#7–9) analyses for CO were performed, but none was detected. In runs 14–17, the buffers were pre-saturated with nitrous oxide. While formaldehyde

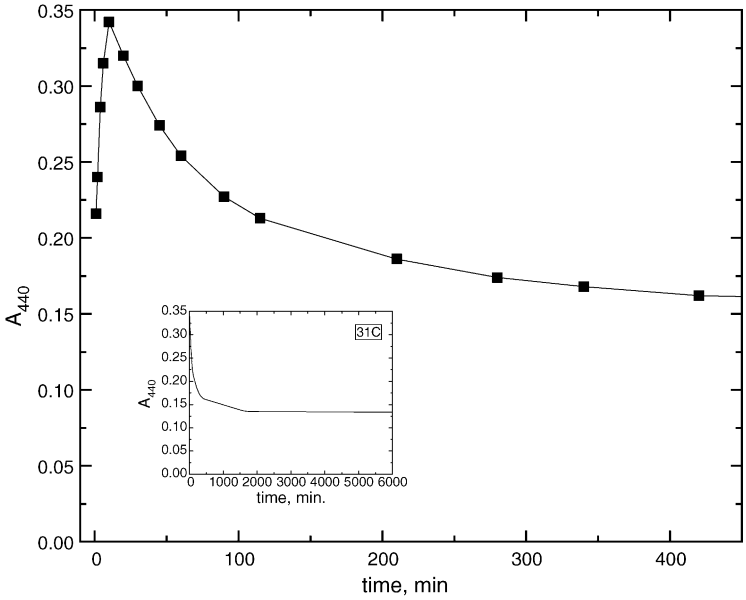

Fig. 2. The time dependence of the absorbance at 440 nm for a pH 6.2 solution (run 31C). The initial absorbance increase over the first 10 min corresponds to elimination of the formaldehyde from $CoHMDCH_2OH^{2+}$; the subsequent decrease over the next few hours corresponds to stage II, hydrogen formation. On a much longer time scale (see inset), over the next day or so, the base-catalyzed isomerization of *N-meso*-$CoHMD^{2+}$ to the *N-rac* isomer [45] is observed.

I. *N-meso*-CoHMD$(CH_2OH)^{2+}$ ⟶ *N-meso*-CoHMD$(H)^{2+}$ + CH_2O

II. *N-meso*-CoHMD$(H)^{2+}$ ⟶ *N-meso*-CoHMD^{2+} + ½ H_2

III. *N-meso*-CoHMD^{2+} ⟶ *N-rac*-CoHMD^{2+}

Scheme 1. Overview.

was produced in high yield, no hydrogen was formed and molecular nitrogen was observed as a product. The errors for the formaldehyde and hydrogen determination are ca. ±15% and greater for dinitrogen because of the need to correct for air leaks.

3.4. Stage I: formaldehyde production

$$\text{I. } N\text{-}meso\text{-CoHMD}(CH_2OH)^{2+} \rightarrow N\text{-}meso\text{-CoHMD}(H)^{2+} + CH_2O$$

Formaldehyde yields under a range of conditions are given in Tables 7 and 9. Individual runs gave good fits to first-order kinetics for stage I. Fig. 3 summarizes the pH dependence of the pseudo first-order rate constants $k_{I,obs}$ determined for the different pH solutions.

Note that the variable ionic strength data points (circles) seem to converge on the other data set at high pH. This is because μ is 0.01–0.02 M for the pH 3–5 circles, but closer to 0.1–0.2 M for the pH 6–7 runs in phosphate buffers. The rate law for stage I is $-d[N\text{-}meso\text{-CoHMD}(CH_2OH)^{2+}]/dt = k_I[N\text{-}meso\text{-CoHMD}(CH_2OH)^{2+}]/[H^+]$, with $k_I = 3.5 \times 10^{-9}\ M\ s^{-1}$ at pH 3–7 and 0.5 M ionic strength. Note that k_I appears to increase about a factor of four upon decreasing μ from 0.5 to 0.01 M, consistent with a decreased charge in the activated complex.

3.5. Stage II: hydrogen production

Kinetic and product yield data were given in Tables 7–10. Hydrogen yields determined in the series of runs at 0.5 M ionic strength approach 0.5, the maximum yield consistent with formation of Co(II) as product. In the runs performed under an atmosphere of N_2O (0.02 M) no hydrogen was found, although formaldehyde was produced in high yield. In addition, molecular nitrogen was produced. This suggests (but does not require, as discussed later) that cobalt(I) (which reacts very rapidly with N_2O [25] to yield Co(III) and N_2) is an intermediate in hydrogen formation. While there are clearly (at least) three reaction stages (Fig. 2), the kinetics of the second stage are rather difficult to disentangle. Both first-order and second-order fits were attempted for the first data set (Table 8), but second-order fits gave the best results for the 0.5 M ionic strength data. Generally the 440-nm data ($\Delta\varepsilon = 330\ M^{-1}\ cm^{-1}$) were used. Data preceding the completion of the second half life for stage I were ignored. An infinity value was estimated for the second stage and the data were fit to second-order, equal concentration kinetics, with the slopes of the plots of $1/[CoH^{2+}]$ versus time determined from a linear regression using Origin™. The values from Table 10 are shown in Fig. 4.

Table 6
Spectral properties of reactants, intermediates and products

Species	λ_{max} (nm)	ε ($M^{-1}\ cm^{-1}$)
N-meso-CoHMD$(CH_2OH)^{2+}$	475	216
	378	448
N-meso-CoHMD$(H)^{2+}$	440	445
N-meso-CoHMD^{2+}	446	120
N-rac-CoHMD^{2+}	443	93

The pH 4.5–8, 0.5 M ionic strength data are consistent with the rate law, $-d[N\text{-}meso\text{-CoHMDH}^{2+}]/dt = k_{II}[N\text{-}meso\text{-CoHMDH}^{2+}]^2/[H^+]$, with $k_{II} = 2.0 \times 10^{-7}\ s^{-1}$. As indicated for the pH 3.5, formate data in Fig. 4, second stage data for pH <4.5 (runs 2, 24, 28) are faster than expected from the above first-order inverse dependence on $[H^+]$ and give better fits to a first-order dependence on the concentration of the cobalt complex. In addition, very little hydrogen was detected in these runs.

3.6. Stage III: isomerization of N-meso-CoHMD^{2+}

The final stage observed via UV–vis spectroscopy resulted in very slow, exponential loss of absorbance at 440 nm. Pseudo first-order rate constants for a few runs are given in Table 10, but the stage was not studied extensively once it was recognized that the process was identical with the hydroxide-ion catalyzed isomerization to the more stable N-*rac* complex studied earlier [45]. The data given are in reasonable agreement with the rate law, $-d[N\text{-}meso\text{-CoHMD}^{2+}]/dt = 6 \times 10^{-12}\ [N\text{-}meso\text{-CoHMD}^{2+}]/[H^+]$, determined previously.

4. Discussion

The X-ray diffraction structural study confirms that the product of the photochemical synthesis

$$Co(NH_3)_5(OC(O)CH_2OH)^{2+} \xrightarrow{h\nu, H^+} {}^{\bullet}CH_2OH + Co_{aq}{}^{2+} + 5NH_4{}^{+} + CO_2$$

$$N\text{-}meso\text{-CoHMD}^{2+} + {}^{\bullet}CH_2OH \rightarrow N\text{-}meso\text{-CoHMD}(CH_2OH)^{2+}$$

Table 7
Product yields for low ionic strength solutions (298 K)

Run no.	Conditions {ionic strength, M}	[Co] (mM)	pH	$Y(H_2CO)$[a]	$Y(H_2)$[a]	Other
1	1 mM $HClO_4$ {0.003}	0.68	3	0.5	0.01	
2	$NaHCO_2/HClO_4$ 02/0.01 M {0.02}	0.63	3.7	0.4	0.1	no CO
3	$NaCH_3CO_2/HClO_4$ 0.02/0.01 M {0.02}	0.65	4.64	0.3	0.4	
4A	NaH_2PO_4/Na_2HPO_4 0.1/0.01 M {0.1}	0.68	5.68	0.9	0.5	
4B	NaH_2PO_4/Na_2HPO_4 0.1/0.01 M {0.1}	0.75	5.68	0.6	0.3	no CO
5	NaH_2PO_4/Na_2HPO_4 0.01/0.01 M {0.25}	0.68	7	1.0	0.5	
6	$NaCD_3CO_2/CF_3SO_3H$ 0.05/0.03 M, D_2O {0.05}	4.23	3.8	0.3		
7	CO_2 sat'd 0.1 M $NaHCO_3$ {0.1}	0.87	6.8	0.6	0.3	no CO
8	CO_2 sat'd 0.01 M $NaHCO_3$ {0.01}	0.87	6	0.5	0.3	no CO
9	CO_2 sat'd 0.03 M $NaHCO_3$ {0.03}	0.68	6.4	0.4	0.2	no CO
10	NaH_2PO_4/Na_2HPO_4 0.1/0.01 M {0.1}	1.52	5.7	0.3	0.3	
11	$NaCH_3CO_2/HClO_4$ 0.02/0.01 M {0.02}	1.51	4.6	0.4	0.2	
13	NaH_2PO_4/Na_2HPO_4 0.01/0.01 M {0.04}	0.87	7	0.4	0.4	N_2, ≤0.2
15	NaH_2PO_4/Na_2HPO_4 0.01/0.01 M+ N_2O {0.04}	0.68	7	0.9	≤0.001	N_2, 0.9 ± 0.3
17	$NaCH_3CO_2/CH_3CO_2H$ 0.01/0.01 M+ N_2O {0.01}	0.91	4.7	n.d.	0.01	N_2, 1 ± 0.3
19	$NaCH_3CO_2/CH_3CO_2H$ 0.01/0.01 M {0.01}	0.93	4.7	n.d.	0.2	N_2, ≤0.1

[a] *Y*, yield is defined as mols formaldehyde or dihydrogen produced divided by the mols of complex used.

Table 8
Rate constants at low ionic strength (298 K)

Run no.	Conditions {ionic strength, M}	[Co] (mM)	pH	k_I (s^{-1})[a]	k_{II} (s^{-1})[a] k_{II} ($M^{-1}s^{-1}$)[b]
1	1 mM $HClO_4$ {0.003}	0.68	3	2×10^{-5}	
2	$NaHCO_2/HClO_4$ 0.02/0.01 M {0.02}	0.63	3.7	7×10^{-5}	6.4×10^{-6}[a] 8.6×10^{-3}[b]
3	$NaCH_3CO_2/HClO_4$ 0.02/0.01 M {0.02}	0.65	4.6	4.4×10^{-4}	3.3×10^{-6}[a] 2.8×10^{-3}[b]
4A	NaH_2PO_4/Na_2HPO_4 0.1/0.01 M {0.1}	0.68	5.7	1.5×10^{-3}	5.5×10^{-5}[a] 5.61×10^{-2}[b]
5	$NaH_2PO_4/Na_2HPO_4$0.01/0.01 M {0.25}	0.68	7.0		5.0×10^{-4}[a]
6[c]	$NaCD_3CO_2/CF_3SO_3H$ 0.05/0.03 M, D_2O {0.05}	4.23	3.8	1.3×10^{-4}[c]	
7	CO_2 sat'd 0.1 M $NaHCO_3$ {0.1}	0.87	6.8		4.0×10^{-4}[a]
8	CO_2 sat'd 0.01 M $NaHCO_3$ {0.01}	0.87	6.0		5.0×10^{-5}[a]
10	$NaH_2PO_4/Na_2HPO_4$0.1/0.01 M {0.1}	1.52	5.7		3.3×10^{-5}[a]
16, 17	$NaCH_3CO_2/CH_3CO_2H$, 0.01/0.01 M + N_2O {0.01}	0.91	4.7		3.5×10^{-4}[a]
		0.8			3.3×10^{-4}[a]
18, 19	$NaCH_3CO_2/CH_3CO_2H$, 0.01/0.01 M {0.01}	0.93	4.7		1.1×10^{-4}[a]
		0.82			0.77×10^{-4}[a] 2.6×10^{-1}[b]
22	NaH_2PO_4/Na_2HPO_4 0.1/0.01 M {0.1}	0.67	5.8		5.8×10^{-2}[d]
23	NaH_2PO_4/Na_2HPO_4 0.05/0.05 M {0.2}	1.1	6.8		5.8×10^{-1}[d]
24	CF_3SO_3Na/H_3PO_4 0.01/0.01 M[e] {0.01}	0.67	2		4.3×10^{-6}[e]
		0.67			4.5×10^{-6}[e]
A	NaH_2PO_4/Na_2HPO_4 0.01/0.01 M {0.04}	0.25	6.7	1.0×10^{-2}[f]	

[a] Pseudo first-order rate constant determined at 520 nm for stage I and 440 nm for stage II.
[b] Pseudo second-order rate constant determined at 440 nm.
[c] Determined from ^1H NMR data.
[d] Determined from H_2 production. Pseudo second-order rate constant.
[e] Initially Co-CH_2OH solution was held at pH 5.8 for 45 min to effect the formaldehyde elimination, then acid was added to take the solution to pH 2 so that the metal hydride reaction could be studied at 440 nm at low pH.
[f] Hand-held stopped flow used to mix reagents.

Table 9
Products at 0.5 M ionic strength (maintained with Na_2SO_4)

Run no.	Conditions {ionic strength, M}	[Co] (mM)	pH	Y (H_2CO)[a]	Y (H_2)[a]
26C	$NaCH_3CO_2/CH_3CO_2H$ 0.02/0.02 M	1.16	4.6	0.9	0.3
27	CF_3SO_3H/Na_2HPO_4 0.001/0.02 M	1.15	6.7	0.8	0.4
				0.8	0.3
29	CF_3SO_3H/Na_2HPO_4 0.001/0.01 M	0.68	7.6	0.9	0.4
		1.3		0.8	0.3
		0.9		1.0	0.3
30	CF_3SO_3H/Na_2HPO_4 0.005/0.02 M	0.7	7.1	0.7	0.4
		1.4		0.7	0.6
31	CF_3SO_3H/Na_2HPO_4 0.015/0.02 M	0.81	6.2	0.6	0.3
		1.62		0.7	0.3
32	$NaCH_3CO_2/CF_3SO_3H$ 0.02/0.004 M	1.18	5.2	1.0	0.7

Table 10
Rate constants at 0.5 M ionic strength (maintained with Na_2SO_4)

Run no.	Conditions {ionic strength, M}	[Co] (mM)	pH	k_I (s^{-1})[a]	k_{II} ($M^{-1}\,s^{-1}$)[b]	k_{III} (s^{-1})[c]
25	$NaCH_3CO_2/CH_3CO_2H$ 0.02/0.001 M	1.33	5.6	4.6×10^{-4}	8.4×10^{-2}	9×10^{-6}
		0.68			4.6×10^{-2}	
26	$NaCH_3CO_2/CH_3CO_2H$ 0.02/0.02 M	0.55	4.5	1.1×10^{-4}	3.8×10^{-3}	
27	CF_3SO_3H/Na_2HPO_4 0.001/0.02 M	0.6	6.7	1.1×10^{-2}	1.7×10^{-1}	
		1.15			2.1×10^{-1}	
28	$NaHCO_2/CF_3SO_3H$ 0.02 M/0.01 M	0.69	3.5	1.2×10^{-5}	2.4×10^{-2}	
		1.32		1.4×10^{-5}	2.3×10^{-2}	
29	CF_3SO_3H/Na_2HPO_4 0.001/0.01 M	1.36	7.6[d]		6.2	2.3×10^{-4}
		0.9			8.7	
30	CF_3SO_3H/Na_2HPO_4 0.005/0.02 M	0.7	7.1		2.5	7×10^{-5}
		1.4			0.9	
31	CF_3SO_3H/Na_2HPO_4 0.015/0.02 M	1.62	6.2		0.7	9×10^{-6}
		0.81			0.5	9×10^{-6}
E	CF_3SO_3H/Na_2HPO_4 0.001/0.02 M	0.69	6.6	1.6×10^{-2}[d]		
		1.33				

[a] Pseudo first-order rate constant determined from spectral changes at 520 nm unless otherwise noted.
[b] Pseudo second-order rate constant determined from spectral changes at 440 nm unless otherwise noted.
[c] Pseudo first-order rate constant determined from spectral changes at 440 nm unless otherwise noted.
[d] Hand-held stopped flow used to mix reagents.

is a six-coordinate alkyl-cobalt(III) complex analogous to the methyl complex. The electronic spectrum of the complex in acidic solution indicates that its six-coordinate structure is maintained, that is, that there is a water molecule trans to the hydroxymethyl group. The position of the lowest energy *d–d* band of the complex, 475 nm, indicates that $-CH_2OH^-$ is a lower field ligand than $-H^-$ (440 nm), $-CO_2^{2-}$ (470 nm), or $-CH_3^-$ (470 nm) [25]. From the ^1H NMR chemical shift data, the $-CH_2OH$ group in the complex (δ 3.58 and ∼3.9, ^{13}C 61.6) more closely resembles the hemiacetal $H_2C(OH)(OCH_3)$, δ 4.64, than formaldehyde, δ 9.50, in methanol solvent [33] and is similar to that we find for $Re(bpy)(CO)_3CH_2OH$ (δ 3.27 ^1H, ^{13}C 69.4) in acetonitrile (Table 1).

4.1. The nature of N-meso-CoHMD$(CH_2OH)^{2+}$ in solution

There is, however, an unusual feature of the NMR spectra. The proton NMR spectra of acidic D_2O solutions feature two resonances at δ 3.58 and ∼3.9 in the region assignable to the methylene protons of the $-CH_2OH$ group although a single resonance at δ 61.6 is observed in the ^{13}C NMR spectrum. The ^1H NMR spectra thus suggest the presence of two species containing the $-CH_2OH$ ligand or that the two $-CH_2OH$ protons are not equivalent. Several possibilities were considered. To assess the possibility of a dimeric $-CH_2OCH_2-$ bridged [30,31] species, the behavior of the sample on a cation exchange resin (Sephadex C-25) was examined; under elution

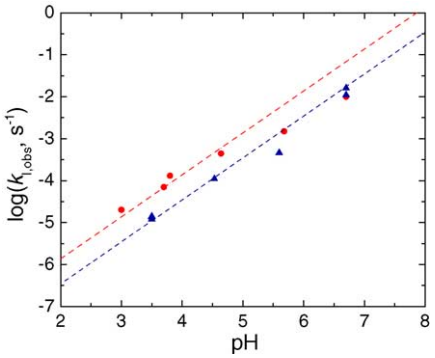

Fig. 3. log($k_{I,obs}$) vs. pH for loss of *N-meso*-CoHMD(CH_2OH)$^{2+}$. Circles, ionic strength variable, 0.01–0.1 M (Table 8); triangles, 0.5 M ionic strength (Na_2SO_4). The lines impose an inverse first-order dependence with $k_I = 1.4 \times 10^{-8}$ M s^{-1} for low ionic strength (solid line) and 3.5×10^{-9} M s^{-1} for high ionic strength (dashed line).

with 0.2 M perchloric or 0.2 M triflic acid, the material's behavior was very similar to that of the methyl complex (charge, +2), which is not consistent with the {Co–CH_2OCH_2–Co}$^{4+}$ hypothesis. An alternative explanation is that there are two configurational isomers with respect to the orientation of the –CH_2OH bond, as has been proposed for a ruthenium complex in the solid state [18] or that hydrogen bonding of the macrocycle N–H to the oxygen atom of the –CH_2OH renders the two methylene protons inequivalent.

4.2. Mechanistic considerations

We have studied the kinetics of three reactions initiated by mixing *N-meso*-CoHMD(CH_2OH)$^{2+}$ with a base. All three exhibit rates that are proportional to the reciprocal of the hydrogen ion concentration. The elimination of formaldehyde via deprotonation of the hydroxymethyl group and the isomerization of the macrocycle via deprotonation of N–H bound to the metal are unremarkable pathways. As discussed in section 1.2, formaldehyde elimination has been observed for other hydroxymethyl complexes of cobalt(III) when the cobalt(I) state is accessible. The formation of H_2 from a metal hydride complex by a base catalyzed path is, however, quite striking. As will be seen, a very important player in the first two reactions is the cobalt(I) complex. A very important additional factor for this system is the macrocycle isomerism as a function of ligand and oxidation state. *N-meso*-CoHMD(H)$^{2+}$ is the most stable isomer of the hydride complexes [25], while *N-rac*-CoHMD^{2+} and *N-rac*-CoHMD^{+} are, respectively, the stable forms of the Co(II) [45] and Co(I) oxidation states [25]. Despite its instability with respect to isomerization, it must be the *N-meso* isomer of Co(I) that is formed from formaldehyde elimination and "later" is active in formation of hydrogen since there is no mechanism for equilibrating the cobalt(I) isomers under these conditions. An electron-transfer mechanism

$$N\text{-}meso\text{-CoHMD}^{+} + N\text{-}rac\text{-CoHMD}^{2+} \rightarrow N\text{-}meso\text{-CoHMD}^{+} + N\text{-}rac\text{-CoHMD}^{2+}$$

is precluded by the absence of *N-rac*-CoHMD^{2+} (formed only on a much longer time scale) and reaction with "water" [25] is not competitive (by many orders of magnitude) with pathways (largely unproductive protonation) that remove *N-meso*-CoHMD^{+}. Relevant rate constants for *N-meso*-CoHMD^{+} protonation reactions are given in Table 3. Given the buffer concentrations used and the tabulated rate constants, it is clear that the lifetime of *N-meso*-CoHMD^{+} produced either via formaldehyde elimination or deprotonation is a microsecond or less.

Rate laws and mechanistic implications for each of the stages will next be discussed in turn.

4.3. Stage I: formaldehyde production

The rate law for stage I is $-$d[*N-meso*-CoHMD(CH_2OH^{2+})]/dt = k_I[*N-meso*-CoHMD(CH_2OH^{2+})]/[H^+], with k_I = $(3.5 \pm 0.5) \times 10^{-9}$ M s^{-1} at pH 3–7 and 0.5 M ionic strength. The rate law is consistent with the elementary steps outlined below in Scheme 2 with $K_1k_2 = (3.5 \pm 0.5) \times 10^{-9}$ M s^{-1} at pH 4–7 and 0.5 M ionic strength. The species *N-meso*-CoHMD(CH_2O)$^{+}$ is formally an aldehyde complex; both σ- and π-bonded aldehyde complexes are known [102]. The value of pK_1 should lie between 16 and 10.7 (the value for the radical [103]) or even below, given the +2 charge of the complex. For pK_1 = 10.7, $k_2 = k_I/K_1 > 10^2$ s^{-1}. The data in Fig. 3 provide no indication of a pK between pH 3 and 7. Despite the low pK found for the hydroxymethyl group bound to NTA (4.7 [40]), it is unlikely that pK_1 is below 3. Protonation of the *N-meso*-CoHMD^{+} produced when formaldehyde is rapidly eliminated should be rapid (see Table 3).

An alternative site for the deprotonation that gives rise to the pH dependence of the rates is the water molecule bound trans to the hydroxymethyl group. This scenario would re-

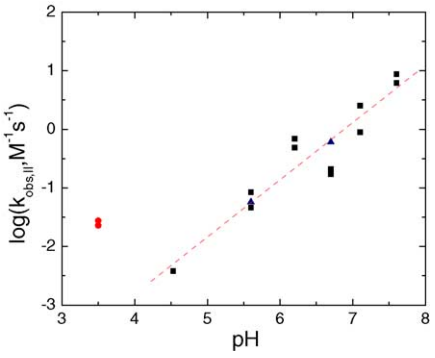

Fig. 4. Pseudo second-order rate constants for stage II (Table 10) for 0.5 M ionic strength as a function of pH. The squares are from treatment of the 440-nm absorbance changes for all but the formate runs (circles). The line is a fit to the data marked with squares gives a first-order inverse dependence on [H^+]. The triangles are for H_2 formation (monitored by GC).

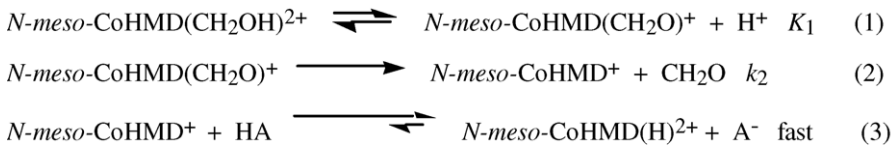

Scheme 2. Stage I formaldehyde elimination mechanism.

quire that release of CH_2OH^+ ($pK < 0$) be accelerated in the hydroxy complex. This mechanism seems unlikely because of the pK_a values required for the trans water molecule and the bound CH_2OH group.

An additional possible pathway for stage I involves homolysis of the Co–C bond, followed by outer-sphere electron transfer from the CH_2OH radical to Co(II) in competition with dimerization of the radical to give ethylene glycol and H-abstraction from *N-meso*-$CoHMDH^{2+}$ (see Scheme 3).

The pK_a of the OH bond in the hydroxymethyl radical is 10.7; the rate constant for dimerization of the radical is $2.4 \times 10^9\ M^{-1}\ s^{-1}$ [103]. The rate constant for H-abstraction from *N-meso*-$CoHMDH^{2+}$ is probably $\sim 1 \times 10^8\ M^{-1}\ s^{-1}$, based on the estimate for the *t*-butanol radical [25]. The reduction potentials for couples involving the $^{\bullet}CH_2OH$ radical have been reported [104,105]:

Base

$CH_2O + e^- = {}^{\bullet}CH_2O^-$; E^0 −1.81 V;

$^{\bullet}CH_2OH + e^- = :CH_2OH^-$ E^0 −0.85 V;

Acid

$CH_2O + H^+ + e^- = {}^{\bullet}CH_2OH$; E^0 −1.18 V

$^{\bullet}CH_2OH + H^+ + e^- = CH_3OH$ E^0 +1.56 V

The reduction potential for $CoHMD^{2+/+}$ is estimated to be −1.32 V versus NHE in water [106] so that reduction of *N-meso*-$CoHMD^{2+}$ to *N-meso*-$CoHMD^+$ by hydroxymethyl radical is thermodynamically favorable in base ($E^0 = -1.81$ V), but not in acid ($E^0 = -1.18$ V).

A homolysis mechanism is not consistent with the observed rate law, specifically a first-order dependence on the concentration of Co-CH_2OH. It is possible, however, that this pathway does contribute to the decomposition of the complex. Because of the complications introduced by stage II, deviations from strictly first-order kinetics could be difficult to recognize. Formaldehyde yields are generally ≪ 100%, being generally smaller at low pH. This could reflect formation of $(CH_2OH)_2$ by reaction 5 and 7.5 and CH_3OH by reaction 7, with the latter becoming more important as the concentration of *N-meso*-$CoHMD(H)^{2+}$ from reaction 3 increases. To the extent that reactions 5 operate there should be a deficit of H_2. Both formaldehyde and hydrogen yields tend to larger values at higher pH consistent with reaction 8 competing more favorably with reactions 5 and 7 as the pH increases. However, the practical problem of analysis of the lower pH solutions where reaction times are very long should also be noted. Long reaction times can lead to slow leakage of air and to H_2 loss from the vessel.

The isomer *N-rac*-$CoHMD(CH_2OH)^{2+}$ (probably the secondary isomer, by analogy with the methyl complex [23]) has been studied in pulse-radiolysis experiments. This hydroxymethyl complex also yields formaldehyde and is reported to decay with a rate constant of $10^{-1}\ s^{-1}$, independent of *N-rac*-$CoHMD(CH_2OH)^{2+}$ and H^+ (pH 1–6) concentrations in the presence of N_2O, which scavenges the *rac* $CoHMD^+$ with a rate constant of $2.5 \times 10^7\ M^{-1}\ s^{-1}$ to give Co(III) and dinitrogen [39]. Thus, there is a remarkable contrast between rates and mechanisms of formaldehyde elimination for the two isomers.

4.4. Stage II: hydrogen production

Hydrogen is produced in stage II.[1] The pH dependence of stage II

II. *N-meso*-$CoHMD(H)^{2+} \rightarrow$ *N-meso*-$CoHMD^{2+} + 1/2H_2$

shown in Fig. 4 is consistent with the rate law

$-d[N\text{-}meso\text{-}CoHMDH^{2+}]/dt = k_{II}[N\text{-}meso\text{-}CoHMDH^{2+}]^2/[H^+]$, with $k_{II} = 2.0 \times 10^{-7}\ s^{-1}$

in the range pH 4.5–8. Scheme 4 gives a reaction sequence consistent with the rate law.

Using a steady-state treatment for the Co(I) complex, one obtains:

$$-\frac{d[CoHMDH^{2+}]}{dt} = \frac{2k_{11}k_{10}[CoHMDH^{2+}]^2}{k_{11}[CoHMDH^{2+}] + k_{-10}[H^+]} \quad (13)$$

In Scheme 4, when the deprotonation of the hydride complex is treated as a pre-equilibrium, i.e., $k_{-10}[H^+] \gg k_{11}[CoHMDH^{2+}]$, then reduction of the hydride complex by its conjugate base, the cobalt(I) complex, is rate determining.

[1] Given that that $CoLH^{2+}$ and formaldehyde are equal in concentrations at the end of stage I, the extent to which the formaldehyde reduction of water contributes to overall hydrogen formation needs to be considered. Formaldehyde decomposition via the Cannizzaro reaction involves disproportionation via reaction of the various hydrated forms [107] viz: $H_2C(OH)_2 + H_2C(O)(OH)^- \rightarrow HCO_2^- + CH_3OH + H_2O$ and parallel formation [108] of H_2 is attributed to hydride transfer from the C-H in the formaldehyde hydrates, e.g. $H_2C(OH)_2 + OH^- \rightarrow H_2 + HCO_2^- + H_2O$ Applying the rate law [108] for relatively low $[OH^-]$, $dH_2/dt = k_{obs}[OH^-]^n[HCHO]^m$ ($m = n = 1$), $k_{obs} = 2.8 \times 10^{-9}\ M^{-1}\ s^{-1}$, for the highest pH studied here, pH 8, the process appears so slow as to contribute negligibly to the observed rate of formation of H_2. Indeed the initial rates reported for 2 M NaOH are orders of magnitude slower than those measured here and formaldehyde can be regarded as quite stable on the timescale of our experiments.

$$\textit{N-meso}\text{-CoHMD}(CH_2OH)^{2+} \rightleftharpoons \textit{N-meso}\text{-CoHMD}^{2+} + \bullet CH_2OH \quad (4)$$

$$2 \bullet CH_2OH \longrightarrow HOCH_2CH_2OH \qquad k = 2.4 \times 10^9\ M^{-1}s^{-1} \quad (5a)$$

$$\bullet CH_2OH + \textit{N-meso}\text{-CoHMD}(CH_2OH)^{2+} \longrightarrow \textit{N-meso}\text{-CoHMD}^{2+} + HOCH_2CH_2OH \quad (5b)$$

$$\bullet CH_2OH \rightleftharpoons \bullet CH_2O^- + H^+ \qquad pK_a = 10.7 \quad (6)$$

$$\bullet CH_2OH + \textit{N-meso}\text{-CoHMDH}^{2+} \longrightarrow \textit{N-meso}\text{-CoHMD}^{2+} + CH_3OH \quad (7)$$

$$\bullet CH_2O^- + \textit{N-meso}\text{-CoHMD}^{2+} \longrightarrow \textit{N-meso}\text{-CoHMD}^{+} + CH_2O \quad (8)$$

$$\textit{N-meso}\text{-CoHMD}^{+} + HA \rightleftharpoons \textit{N-meso}\text{-CoHMD}(H)^{2+} + A^- \quad \text{fast} \quad (3)$$

Scheme 3. Stage I homolysis mechanism.

$$\textit{N-meso}\text{-CoHMD}(H)^{2+} \rightleftharpoons \textit{N-meso}\text{-CoHMD}^{+} + H^+ \qquad k_{10}, k_{-10}, K_{10} \quad (10)$$

$$\textit{N-meso}\text{-CoHMD}^{+} + \textit{N-meso}\text{-CoHMD}(H)^{2+} \longrightarrow \textit{N-meso}\text{-CoHMD}^{2+} + \textit{N-meso}\text{-CoHMD}(H)^{+} \quad k_{11} \quad (11)$$

$$\textit{N-meso}\text{-CoHMD}(H)^{+} + H^+ \longrightarrow \textit{N-meso}\text{-CoHMD}^{2+} + H_2 \qquad \text{fast} \quad (12)$$

Scheme 4.

Molecular hydrogen is formed in a subsequent, rapid step. The pK_a of *N-meso*-CoHMD(H)$^{2+}$ is 12.7 or higher [25]; thus $K_{10} \leq 2 \times 10^{-13}$ M. In terms of Scheme 4, $k_{II} = 2K_{10}k_{11}$ and k_{11} is then $\geq 10^6\ M^{-1}\ s^{-1}$. An upper limit for k_{11} is obtained from the fact that no H_2 is found when the reactant solution is saturated with nitrous oxide.[2]

$$\textit{N-meso}\text{-CoHMD}^{+} + N_2O \rightarrow Co^{III}HMD + N_2 \quad k_{N_2O} \quad (14)$$

Nitrous oxide competes successfully with *N-meso*-CoHMD(H)$^{2+}$ for oxidation of CoHMD$^+$, i.e., $k_{N_2O}[N_2O] = 2.3 \times 10^5\ s^{-1} > k_{11}[\textit{N-meso}\text{-CoHMD}(H)^{2+}]$, k_{11} is then $<10^9\ M^{-1}\ s^{-1}$. Such a large rate constant for electron transfer to the hydride complex is striking, as is the high rate required for the following process.

We note that the reduction of protons by cobaltocene conforms to a mechanism analogous to Scheme 4 (see Section 1.4), with the difference that the relevant hydride is a very strong acid and its formation by proton transfer is relatively slow [87]. For a Rh porphyrin system the reductant analogous to Co(I) is the electrode [89]. In the present system, when the rate of oxidation of Co(I) becomes comparable to or greater than its rate of protonation, i.e., $k_{11}[\text{CoHMDH}^{2+}] \gg k_{-10}[H^+]$, the kinetics will exhibit a smaller dependence on the concentration of the hydride, with the limiting behavior giving the rate law, $-d[\textit{N-meso}\text{-CoHMDH}^{2+}]/dt = k_{10}[\textit{N-meso}\text{-CoHMDH}^{2+}]/[H^+]$.

[2] An alternative sequence that does not involve Co(I) could involve deprotonation of either the water ligand trans to the hydride or of the macrocycle N–H, followed by reaction of this conjugate base with the parent hydride complex. The scavenging of Co(I) by nitrous oxide would then simply represent a side-reaction.

It should be noted that reaction 10 is a shorthand notation for

$$\textit{N-meso}\text{-CoHMD}(H)^{2+} + A^- \rightarrow \textit{N-meso}\text{-CoHMD}^{+} + HA\ K_{10} \quad (10')$$

where HA may be any of the acids present in the solution (H_3O^+, HAc, $H_2PO_4^-$; Table 3), with A^-, its conjugate base [25]. Thus, the term, $k_{10}[\textit{N-meso}\text{-CoHMDH}^{2+}]/[H^+]$ is actually a sum of contributions, $k_{10,i}[\textit{N-meso}\text{-CoHMDH}^{2+}][A_i^-]$, for all bases A_i^- present. We have not developed this point at length, because the individual deprotonation rate constants are not known, since only a limit for pK_{10} is available. This is an important feature of the system, however, because it is the actual concentrations of kinetic bases present (not simply the hydrogen ion concentration) and their rate constants that determine whether a pre-equilibrium obtains (second-order kinetics) or whether deprotonation of the hydride is rate determining (first-order kinetics). This feature may account for the difficulty in determining whether the runs in Table 7 follow a first or second-order dependence on [*N-meso*-CoHMD(H)$^{2+}$].

5. Conclusions

The complexes *N-meso*-CoHMD(CH$_2$OH)$^{2+}$ and *N-meso*-CoHMD(H)$^{2+}$ are consistently described as six-coordinate coordination complexes of cobalt(III) in which the four macrocycle nitrogen atoms occupy a plane and CH_2OH^- or H^- ligands occupy axial coordination positions, with the sixth coordination site occupied by a trans H_2O ligand. Aqueous solutions of both are fairly stable in acid (order of a day)

and both decompose by pathways inverse in the hydrogen ion concentration. For the case of the hydroxymethyl complex, the postulated mechanism involves proton loss from the hydroxyl group of the hydroxymethyl complex, followed by elimination of formaldehyde. For the case of the hydride complex, the proposed mechanism consists of deprotonation of the metal hydride bond to yield the Co(I) complex, followed by reduction of the parent hydride and rapid formation of Co(II) and H_2. While such a pathway is not without precedent, its operation in alkaline solution is particularly striking since the thermodynamics for H_2 formation become less and less favorable as the pH increases [27].

6. Supplementary material

Crystallographic data have been deposited with the Cambridge Crystallographic Data Centre (deposition number CCDC 230101). Copies of the data can be obtained free of charge from The Director CCDC, 12 Union Road, Cambridge CB21EZ, UK. E-mail: deposit@ccdc.cam.uk.

Acknowledgments

This research was carried out at Brookhaven National Laboratory under contract DE-AC02-98CH10884 with the U.S. Department of Energy and supported by its Division of Chemical Sciences, Office of Basic Energy Sciences. We thank Carolyn Schwarz for teaching us the intricacies of isomerism in this series and for conducting the NMR studies, Bruce S. Brunschwig for help with the kinetics experiments, and Morris Bullock, Robert T. Hembre, Norman Sutin and Harold A. Schwarz for helpful discussions.

References

[1] N. Shaham, H. Cohen, R.V. Eldik, D. Meyerstein, J. Chem. Soc. Dalton Trans. 2000 (2000) 3356.
[2] J.K. Kochi, Organometallic Mechanisms and Catalysis, Academic Press, NY, 1978.
[3] R. van Eldik, D. Meyerstein, Acc. Chem. Res. 33 (2000) 207.
[4] J. Espenson, in: A.G. Sykes (Eds.), Advances in Inorganic and Bioinorganic Mechanisms, 1982, p. 1.
[5] J.H. Espenson, Prog. Inorg. Chem. 30 (1983) 189.
[6] J.H. Espenson, Acc. Chem. Res. 25 (1992) 222.
[7] D. Meyerstein, Acc. Chem. Res. 11 (1978) 43.
[8] A. Bakac, J.H. Espenson, J. Am. Chem. Soc. 108 (1986) 713.
[9] R. Guilard, K.M. Kadish, Chem. Rev. 88 (1988) 1121.
[10] T.S. Roche, J.F. Endicott, Inorg. Chem. 13 (1974) 1575.
[11] T.S. Roche, J.F. Endicott, J. Am. Chem. Soc. 94 (1972) 8622.
[12] A. Bakac, J.H. Espenson, Inorg. Chem. 28 (1989) 4319.
[13] A. Bakac, J.H. Espenson, Inorg. Chem. 26 (1987) 4353.
[14] D.D. Campano, E.R. Kantrowitz, M.Z. Hoffman, M.S. Weinberg, J. Phys. Chem. 78 (1974) 686.
[15] A.M. Tait, M.Z. Hoffman, E. Hayon, Int. J. Rad. Phys. Chem. 8 (1976) 691.
[16] A.M. Tait, M.Z. Hoffman, E. Hayon, J. Am. Chem. Soc. 98 (1976) 86.
[17] H. Nagao, T. Mizulawa, K. Tanaka, Inorg. Chem. 33 (1994) 3415.
[18] K. Toyohara, K. Tsuge, K. Tanaka, Organometallics 14 (1995) 5099.
[19] A.R. Cutler, P.K. Hanna, J.C. Vites, Chem. Rev. 88 (1988) 1363.
[20] E. Fujita, D.J. Szalda, C. Creutz, N. Sutin, J. Am. Chem. Soc. 110 (1988) 4870.
[21] E. Fujita, D.J. Szalda, Inorg. Chim. Acta 297 (2000) 139.
[22] D.J. Szalda, E. Fujita, C. Creutz, Inorg. Chem. 28 (1989) 1446.
[23] D.J. Szalda, C.L. Schwarz, C. Creutz, Inorg. Chem. 30 (1991) 586.
[24] C. Creutz, H.A. Schwarz, J.F. Wishart, E. Fujita, N. Sutin, J. Am. Chem. Soc. 111 (1989) 1153.
[25] C. Creutz, H.A. Schwarz, J.F. Wishart, E. Fujita, N. Sutin, J. Am. Chem. Soc. 113 (1991) 3361.
[26] G.M. Brown, B.S. Brunschwig, C. Creutz, J.F. Endicott, N. Sutin, J. Am. Chem. Soc. 101 (1979) 1298.
[27] N. Sutin, C. Creutz, E. Fujita, Comments Inorg. Chem. 19 (1997) 67.
[28] U. Koelle, N. J. Chem. 16 (1992) 157.
[29] J.A. Roth, M. Orchin, J. Organomet. Chem. 172 (1979) C27.
[30] C.P. Casey, M.A. Andrews, D.R. McAlister, J.E. Rinz, J. Am. Chem. Soc. 102 (1980) 1927.
[31] G.D. Vaughn, J.A. Gladysz, J. Am. Chem. Soc. 103 (1981) 5608.
[32] G.D. Vaughn, J.A. Gladysz, Organometallics 3 (1984) 1596.
[33] D.H. Gibson, B.A. Sleadd, X. Yin, A. Vij, Organometallics 17 (1998) 2689.
[34] C. Lapinte, D. Catheline, D. Astruc, Organometallics 7 (1988) 1683.
[35] S.L. Van Voorhees, B.B. Wayland, Organometallics 4 (1985) 1887.
[36] M. Wei, B.B. Wayland, Organometallics 15 (1996) 4681.
[37] X. Fu, L. Basickes, B.B. Wayland, J. Chem. Soc. Chem. Commun. (2003) 520.
[38] X. Fu, B.B. Wayland, J. Am. Chem. Soc. 126 (2004) 2623.
[39] H. Elroi, D. Meyerstein, J. Am. Chem. Soc. 100 (1978) 5540.
[40] D. Meyerstein, H.A. Schwarz, J. Chem. Soc. Faraday Trans. I 84 (1988) 2933.
[41] H. Cohen, D. Meyerstein, Inorg. Chem. 13 (1974) 2434.
[42] W. Schmidt, J.H. Swinehart, H. Taube, J. Am. Chem. Soc. 93 (1971) 1117.
[43] A. Rotman, H. Cohen, D. Meyerstein, Inorg. Chem. 24 (1985) 4158.
[44] D.P. Rillema, J.F. Endicott, E. Papaconstantinou, Inorg. Chem. 10 (1971) 1739.
[45] D.J. Szalda, C.L. Schwarz, J.F. Endicott, E. Fujita, C. Creutz, Inorg. Chem. 28 (1989) 3214.
[46] A. Bakac, J.H. Espenson, J. Am. Chem. Soc. 106 (1984) 5197.
[47] G.N. Schrauzer, A. Ribeiro, L.P. Lee, R.K.Y. Ho, Angew. Chem. Int. Ed. Engl. 10 (1971) 807.
[48] M. Masarwa, H. Cohen, R. Glaser, D. Meyerstein, Inorg. Chem. 29 (1990) 5031.
[49] H. Cohen, D. Meyerstein, Inorg. Chem. 27 (1988) 3429.
[50] H. Ogino, M. Shimura, N. Tanaka, Inorg. Chem. 21 (1982) 126.
[51] H. Cohen, D. Meyerstein, J. Chem. Soc. Dalton Trans. (1974) 2559.
[52] L.I. Simhndi, E. Budo-Zahonyi, Z. Szeverenyi, Inorg. Nucl. Chem. Lett. 12 (1976) 237.
[53] J. Halpern, I.G.D. Venerable, J. Am. Chem. Soc. 93 (1971) 2176.
[54] F.C. Anson, H.S. Lim, Inorg. Chem. 10 (1971) 103.
[55] S.S. Kristjánsdóttir, J.R. Norton, J. Am. Chem. Soc. 113 (1991) 4366.
[56] S.S. Kristjánsdóttir, J.R. Norton, in: A. Dedieu (Ed.), Transition Metal Hydrides, VCH, New York, 1992, p. 309.
[57] C.J. Curtis, A. Miedaner, W.W. Ellis, D.L. DuBois, J. Am. Chem. Soc. 124 (2002) 1918.
[58] C.J. Curtis, A. Miedaner, R. Ciancanelli, W.W. Ellis, B.C. Noll, M. Rakowski DuBois, D.L. DuBois, Inorg. Chem. 42 (2003) 216.

[59] C.J. Curtis, A. Miedaner, J.W. Raebiger, D.L. DuBois, Organometallics 23 (2004) 511.
[60] E. Fujita, J.F. Wishart, R. van, Eldik. Inorg. Chem. 41 (2002) 1579.
[61] T. Ramasami, J.H. Espenson, Inorg. Chem. 19 (1980) 1846.
[62] C. Creutz, H.A. Schwarz, N. Sutin, J. Am. Chem. Soc. 106 (1984) 3036.
[63] F. Shafiq, D.J. Szalda, C. Creutz, R.M. Bullock, Organometallics 19 (2000) 824.
[64] D.E. Cabelli, F. Shafiq, C. Creutz, R.M. Bullock, Organometallics 20 (2001) 3729.
[65] D.J. Evans, C.J. Pickett, Chem. Soc. Rev. 32 (2003) 268.
[66] N. Sutin, C. Creutz, E. Fujita, Comments Inorg. Chem. 19 (1997) 67.
[67] B.R. James, Homogeneous Hydrogenation, John Wiley & Sons, New York, 1973.
[68] P.A. Chaloner, M.A. Esteruelas, F. Joó, L.A. Oro, Homogeneous Hydrogenation, Kluwer Academic Publishers, Boston, 1994.
[69] B. De Vries, J. Catal. 1 (1962) 489.
[70] M.G. Burnett, P.J. Connolly, C. Kemball, J. Chem. Soc. A (1967) 800.
[71] G.J. Kubas, Acc. Chem. Res. 21 (1988) 120.
[72] P.G. Jessop, R.H. Morris, Coord. Chem. Rev. 121 (1992) 155.
[73] S.G. Yan, B.S. Brunschwig, C. Creutz, E. Fujita, N. Sutin, J. Am. Chem. Soc. 120 (1998) 10553.
[74] K. Zhang, A.A. Gonzalez, C.D. Hoff, J. Am. Chem. Soc. 111 (1989) 3627.
[75] D.A. Ryan, J.H. Espenson, Inorg. Chem. 20 (1981) 4401.
[76] T.-H. Chao, J.H. Espenson, J. Am. Chem. Soc. 100 (1978) 129.
[77] P. Connolly, J.H. Espenson, Inorg. Chem. 25 (1986) 2684.
[78] U. Koelle, M. Graetzel, Angew. Chem. Int. Ed. Engl. 26 (1989) 567.
[79] U. Koelle, B.S. Kang, P.P. Infelta, P. Compte, M. Graetzel, Chem. Berl 122 (1989) 1869.
[80] J.-M. Lehn, J.-P. Sauvage, Nouv. J. Chim. 1 (1977) 449.
[81] G.M. Brown, S.F. Chan, C. Creutz, H.A. Schwarz, N. Sutin, J. Am. Chem. Soc. 101 (1979) 7638.
[82] S.F. Chan, M. Chou, C. Creutz, T. Matsubara, N. Sutin, J. Am. Chem. Soc. 103 (1981) 369.
[83] Q.G. Mulazzani, M.Z. Silvano Emmi, M. Hoffman, Venturi, J. Am. Chem. Soc. 103 (1981) 3362.
[84] Q.G. Mulazzani, M. Venturi, M.Z. Hoffman, J. Phys. Chem. 86 (1982) 242.
[85] C. Creutz, A.D. Keller, N. Sutin, A.P. Zipp, J. Am. Chem. Soc. 104 (1982) 3618.
[86] M. Chou, C. Creutz, D. Mahajan, N. Sutin, A.P. Zipp, Inorg. Chem. 21 (1982) 3989.
[87] U. Koelle, P.P. Infelta, M. Graetzel, Inorg. Chem. 27 (1988) 879.
[88] U. Koelle, S. Paul, Inorg. Chem. 25 (1986) 2689.
[89] V. Grass, D. Lexa, J.M. Saveant, J. Am. Chem. Soc. 119 (1997) 7526.
[90] I. Bhugun, D. Lexa, J.M. Saveant, J. Am. Chem. Soc. 118 (1996) 3982.
[91] R.M. Kellett, T.G. Spiro, Inorg. Chem. 24 (1985) 2373.
[92] J.P. Collman, Y.Y. Ha, P.S. Wagenknecht, M.A. Lopez, R. Guilard, J. Am. Chem. Soc. 115 (1993) 9080.
[93] C.C. Etsuko Fujita, N. Sutin, D.J. Szalda, J. Am. Chem. Soc. 113 (1991) 343.
[94] H.A. Schwarz, C. Creutz, N. Sutin, Inorg. Chem. 24 (1985) 433.
[95] R.D. Butler, H. Taube, J. Am. Chem. Soc. 87 (1965) 5597.
[96] N.E. Katz, D.J. Szalda, M.H. Chou, C. Creutz, N. Sutin, J. Am. Chem. Soc. 111 (1989) 6591.
[97] C.E. Bricker, W.A. Vail, Anal. Chem. 22 (1950) 664.
[98] International Tables for X-ray Crystallography, vol. I, Kynoch Press, Birmingham, UK, 1969.
[99] L.G. Warner, N.J. Rose, D.H. Busch, J. Am. Chem. Soc. 90 (1968) 6938.
[100] M.J. Heeg, J.F. Endicott, M.D. Glick, Inorg. Chem. 20 (1981) 1196.
[101] J.F. Endicott, J. Lilie, J.M. Kuszaj, B.S. Ramawamy, W.J. Schmonsees, M.G. Simic, M.D. Glick, D.P. Rillema, J. Am. Chem. Soc. 99 (1977) 429.
[102] N.Q. Mendez, J.W. Seyler, A.M. Arif, J.A. Gladysz, J. Am. Chem. Soc. 115 (1993) 2323.
[103] M. Simic, P. Neta, E. Hayon, J. Phys. Chem. 73 (1969) 3794.
[104] H.A. Schwarz, R.W. Dodson, J. Phys. Chem. 93 (1989) 409.
[105] V.A. Benderskii, A.V. Benderskii, Laser Electrochemistry of Intermediates, CRC Press, Boca Raton, 1995.
[106] E. Fujita, C. Creutz, N. Sutin, D.J. Szalda, J. Am. Chem. Soc. 113 (1991) 343.
[107] R.J.L. Martin, Aust. J. Chem. 7 (1954) 335.
[108] S. Kapoor, F.A. Barnabas, J.M.C. Sauer, D. Meisel, C.D. Jonah, J. Phys. Chem. 99 (1995) 6857.